Available online at www.sciencedirect.com
SCIENCE DIRECT
Acta Materialia 54 (2006) 167–172
Acta MATERIALIA
www.actamat-journals.com

Temperature influence on the faceting of $\Sigma 3$ and $\Sigma 9$ grain boundaries in Cu

B.B. Straumal [a,*], S.A. Polyakov [a,b], E.J. Mittemeijer [b]

[a] Institute of Solid State Physics, Laboratory of Interfaces in Metals, Russian Academy of Sciences, Institutskii Prospect 15, 142432 Chernogolovka, Moscow District, Russia
[b] Max-Planck-Institut für Metallforschung and Institut für Metallkunde, Heisenbergstr. 3, 70569 Stuttgart, Germany

Received 12 May 2005; received in revised form 12 July 2005; accepted 25 August 2005
Available online 11 October 2005

Abstract

The faceting of a tube-like tilt grain boundary (GB) in Cu bicrystals has been studied in the temperature interval from 0.5 to 0.95 of the melting temperature T_m ($T_m = 1356$ K). The grains of the bicrystals form the coincidence site lattice (CSL) with inverse density of coincidence sites $\Sigma = 3$ and $\Sigma = 9$. No rounded edges between facets were observed up to $0.95T_m$. With decreasing temperature new facets of increasingly higher CSL indices appear. At $0.5T_m$ six crystallographically different $\Sigma = 3$ facets exist simultaneously. The appearance of high-index CSL facets can be explained by the roughening phase transition of a Kosterlitz–Thouless type. The ratio of GB energy σ_{GB} and surface energy σ_{sur} of the specimen was measured by applying atomic force microscopy to the profile of the GB thermal groove formed upon additional annealing. The Wulff–Herring diagrams were constructed using measured σ_{GB}/σ_{sur} values.

Keywords: Grain boundaries; Faceting; Roughening; Cu; Phase diagrams

1. Introduction

High-angle grain boundaries (GBs) are those with misorientation angles θ above 15°. They cannot be described as an array of lattice dislocations because at high θ the dislocation cores merge. At certain misorientations θ_Σ, called coincidence misorientations, a part of the lattice sites of the lattice 1 coincide with the lattice sites of the lattice 2, forming a coincidence site lattice (CSL) [1]. A CSL is characterized by a parameter Σ (Σ being the inverse density of coincidence sites). At exactly θ_Σ GBs have a perfect periodic structure. These coincidence GBs possess extreme properties like low energy σ_{GB}, migration rate, diffusion permeability and high strength, see [4] and references therein. The coincidence GBs also tend to facet. A curved GB breaks by faceting into an array of flat segments. These segments are frequently parallel to those CSL planes which are densely packed with coincidence sites. Strictly speaking, a CSL exists only at exactly θ_Σ. Any low deviation $\Delta\theta = |\theta - \theta_\Sigma|$ destroys the geometrical coincidence of lattice sites. However, a near-coincidence GB tends to conserve its low-energy structure up to a certain $\Delta\theta$. The structure of such (special) GBs consists of portions of perfectly coincident lattices separated be the intrinsic GB dislocations (IGBDs) [2]. The IGBDs have a Burgers vector b_Σ. b_Σ is shorter than a Burgers vector of lattice dislocations b: $b_\Sigma = b\Sigma^{-2}$. It has been demonstrated that the special GBs conserve their special structure and properties up to a certain critical misorientation $\Delta\theta_c$ and temperature T_c [3]. $\Delta\theta_c$ decreases exponentially and T_c decreases parabolically with increasing Σ [4]. In other words, with decreasing temperature, more GBs with higher Σ result in special structures and properties.

The physical reason for such behavior can be the GB faceting-roughening phase transformation similar to that of free surfaces [5–7]. The free energy of individual steps in a flat surface facet decreases with increasing

* Corresponding author. Tel.: +7 095 6768673; fax: +7 095 2382326.
E-mail address: straumal@issp.ac.ru (B.B. Straumal).

1359-6454/$30.00
doi:10.1016/j.actamat.2005.08.037

temperature. At a certain temperature T_R a step energy becomes zero. If $T_R < T_m$ (T_m is the melting temperature) the flat facet cannot be stable above T_R due to the spontaneous formation of step arrays and becomes rough (roughening transition) [8]. The GB roughening transition has been observed in SrTiO3 between 1773 and 1873 K [9]. The GB roughening transition of second order has been observed recently in Mo [10]. It has been predicted theoretically that the T_R is lower for the facets with higher step energy (i.e., for the facets less densely packed with lattice sites) [8]. Experimentally, a sequence of three roughening transitions for different surface facets at different T_R has only been observed in solid helium [11].

CSL plays a role for GBs similar to that of the crystal lattice for free surfaces. Therefore, one can expect that with decreasing temperature, new GB facets with decreasing density of coincidence sites can appear [9,12] similar to how the GBs with high Σ become special at low temperature [4].

2. Experimental

For the investigation of GB faceting, a cylindrical Cu bicrystal with two coaxial grains was grown by the Bridgman technique from Cu of 99.999 wt.% purity. The grain 1 in this bicrystal is completely surrounded by the co-axial grain 2 forming the $\Sigma9$ $\langle 1\,1\,0\rangle$ tilt GB. The $\{1\,1\,1\}/\{1\,1\,5\}$ inclination of the $\Sigma9$ GB is unstable against the dissociation reaction: $\Sigma9 \rightarrow \Sigma3 + \Sigma3$. Therefore, elongated twins (Fig. 1) with well developed $\Sigma3$ GBs appear during the growth of bicrystal, instead of $\{1\,1\,1\}_1/\{1\,1\,5\}_2$ [or $(1\,1\,0)_{\Sigma9CSL}$] facets (the subscripts 1 and 2 correspond to the grains 1 and 2) [11]. The $\langle 1\,1\,0\rangle$ axes in both grains are parallel to the growth axis. Therefore, the $\Sigma3$ $\langle 1\,1\,0\rangle$ tilt GB in the cylindrical sample with $\langle 1\,1\,0\rangle$ cylinder axis contains all crystallographically possible inclinations. 2.5 mm thick platelets were cut from the grown bicrystal perpendicular to the growth axis. $\Sigma3$ and $\Sigma9$ GBs are normal to both sample surfaces. The platelets were ground with 4000 SiC paper and polished with 3 and 1 μm diamond paste. After that they were annealed in 80% Ar + 20% H_2 gas mixture (purity of gases was 99.999%) at pressure of 2×10^4 Pa at different temperatures and times (1293 K, 48 h; 1073 K, 2374 h; 973 K, 4320 h; 923 K, 4320 h; 873 K, 2391 h; 673 K, 6480 h). During the annealing the GBs migrate slowly (10^{-10}–10^{-13} m/s) under the action of capillary driving force. The GB migration permits the facets to develop which are in equilibrium at the respective annealing temperatures. The annealed samples were than etched in 50% HNO_3 aqueous solution. The GB shape was photographed in polarized light in bright and dark field with the aid of an Zeiss Axiophot optical microscope. The sample annealed at 1293 K was then carefully repolished and annealed 48 h once again in order to form GB thermal grooves. The profiles of the GB thermal groove formed were analysed with the aid of the Topometrix 2000 Explorer atomic force microscope (AFM) operating in the contact mode. The typical field analyzed with the aid of AFM had dimensions of 50×50 μm containing 500×500 pixels. For the analysis, 10 neighboring profiles were used to obtain a mean GB groove profile. The ratio between GB energy σ_{GB} and surface energy σ_{sur} was calculated from the relation $\sigma_{GB} = 2\sigma_{sur}\cos\frac{\alpha}{2}$ using the values of the measured GB groove angles α [13]. This simplified equation is derived from the Herring condition for local equilibrium that balances the tangential and normal (torques) forces at a triple line. To reach the equation above, the torques were assumed to be zero. This approximation is normally used for metals with a face-centered cubic (fcc) lattice since their surfaces are nearly isotropic [11–14]. In addition, the GB is always normal to the sample surface, the groove angle α is close to 180° and the groove surface is continuously curved (it does not contain any facets). GB torques may be significant close to the intersections of GB facets. Therefore, the groove angle α has been measured far away from GB facet edges. The distance from an intersection of GB facets to the measurement place was at least $10^2 w$, where w is a groove width. For the determination of the groove angle not only the groove tip but the full groove profile was used [15].

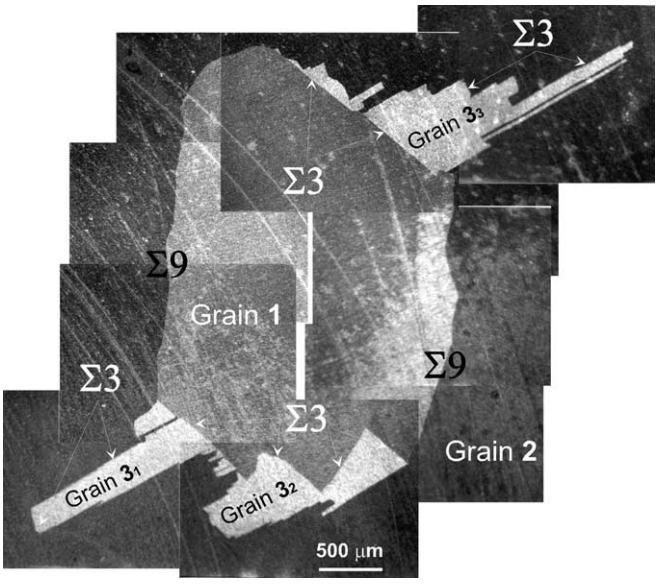

Fig. 1. The section of the as grown bicrystal with $\Sigma9$ $\langle 1\,1\,0\rangle$ tilt GB. The grain 1 is completely surrounded by the grain 2. Close to the $\{1\,1\,1\}_1/\{1\,1\,5\}_2$ inclination the $\Sigma9$ GB dissociates into two $\Sigma3$ GBs (the subscripts 1 and 2 correspond to the grains 1 and 2). Positions of the $\Sigma9$ and $\Sigma3$ GBs are shown.

3. Results and discussion

At $T = 1293\ \mathrm{K} = 0.95T_m$ (i.e., very close to the melting temperature) two facets appear at the $\Sigma3$ GB: $\{1\,1\,1\}_1/\{1\,1\,1\}_2$ or $(1\,0\,0)_{CSL}$ and 9R. Their crystallography is shown in Fig. 2(a). The Wulff–Herring plot with σ_{GB}/σ_{sur} ratios for both facets measured by thermal grooves is shown in Fig. 3. In this plot the interface free energy per unit area $f(\boldsymbol{m})$ is drawn as a polar plot (Wulff plot,

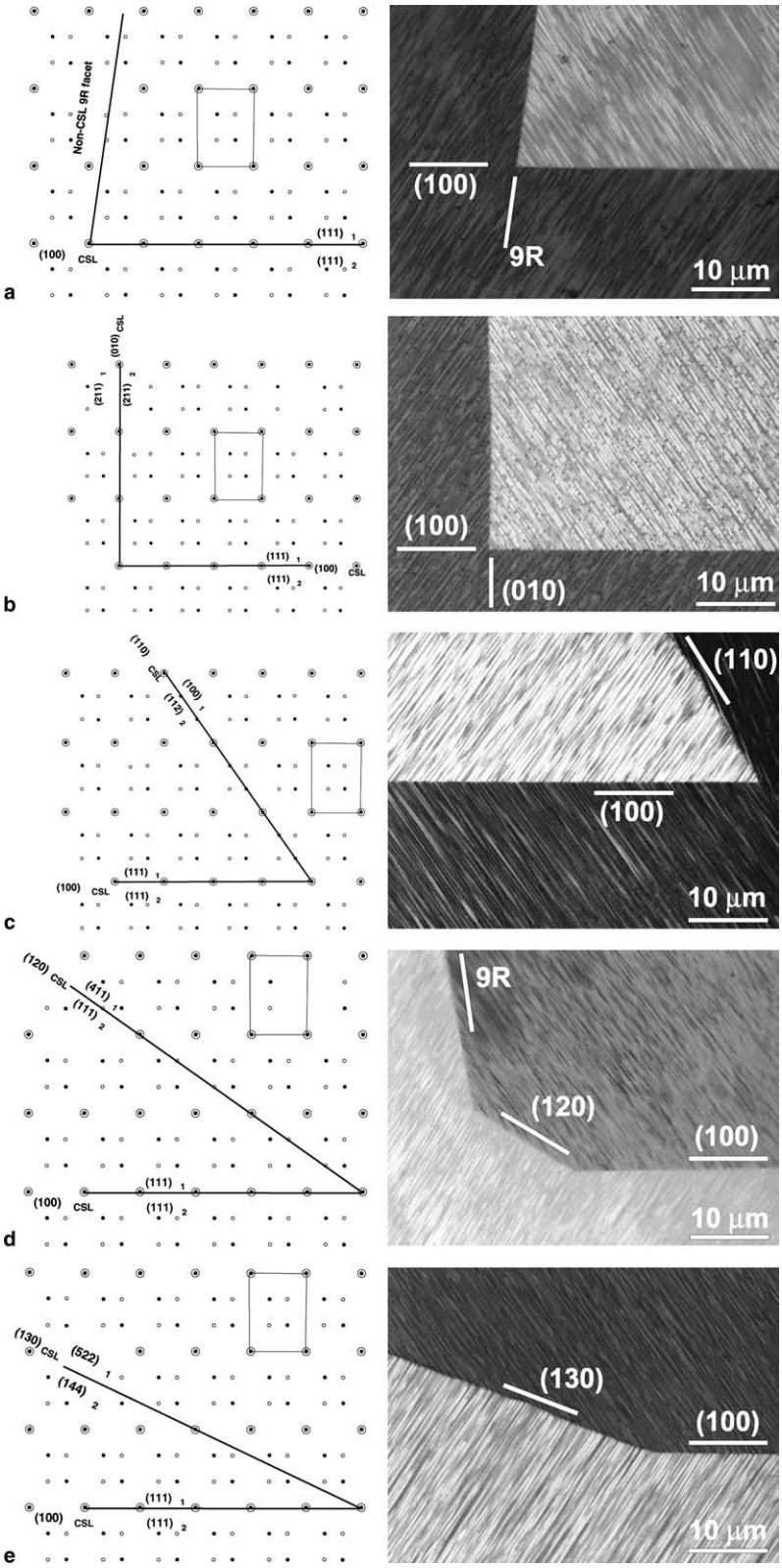

Fig. 2. Sections of Σ3 CSL perpendicular to the {1 1 0} tilt axis with position of various facets (left) and micrographs of intersections of $(1\,0\,0)_{CSL}$ with other facets (right). (a) $(1\,0\,0)_{CSL}$ and 9R facets, 1293 K; (b) $(1\,0\,0)_{CSL}$ and $(0\,1\,0)_{CSL}$ facets, 673 K; (c) $(1\,0\,0)_{CSL}$ and $(1\,1\,0)_{CSL}$ facets, 923 K; (d) $(1\,0\,0)_{CSL}$ and $(1\,2\,0)_{CSL}$ facets, 973 K; (e) $(1\,0\,0)_{CSL}$ and $(1\,3\,0)_{CSL}$ facets, 673 K. The lattice indexes are also given for all CSL facets.

sometimes called γ plot). The shape of $f(\boldsymbol{m})$ (solid line) between measured values for the GB facets (open circles) is shown schematically. One obtains the crystal shape $r(\boldsymbol{h})$ from $f(\boldsymbol{m})$ as the interior envelope of the family of perpendicular planes passing through the end of radius-vectors in each point of $f(\boldsymbol{m})$. Such a crystal shape corresponds to the

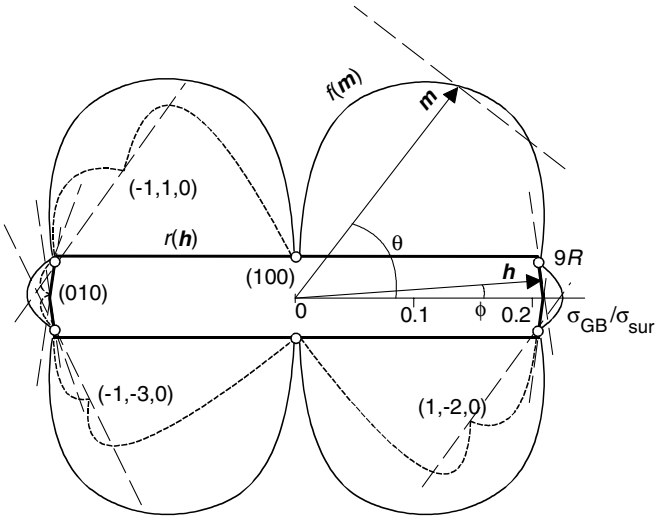

Fig. 3. Wulff–Herring energy $f(\boldsymbol{m})$ (thin solid line) and resulting ECS $r(\boldsymbol{h})$ (thick solid line) in plane section perpendicular to the {110} tilt axis for the Σ3 GBs in Cu at 1293 K. Open circles represent the GB energy σ_{GB} for the $(100)_{CSL}$ and 9R facets measured with the aid of AFM. θ and ϕ are angular variables which measure interfacial orientation ($\boldsymbol{m}$) and crystal shape ($\boldsymbol{h}$), respectively. The cusps (dashed thin curves) for the $\{211\}_1/\{211\}_2$ or $(010)_{CSL}$, $\{100\}_1/\{112\}_2$ or $(110)_{CSL}$, $\{411\}_1/\{111\}_2$ or $(120)_{CSL}$ and $\{522\}_1/\{144\}_2$ or $(130)_{CSL}$ facets with perpendicular planes touching the $r(\boldsymbol{h})$ are also shown.

minimum of the free energy. σ_{GB} of $\{111\}_1/\{111\}_2$ or $(100)_{CSL}$ (symmetric twin GB) is very low, and therefore, according to the Wulff plot, the resultant equilibrium crystal shape (ECS) corresponds to the well known shape of elongated thin twin plates in Cu. However, the ECS differs from the GB shape shown in Fig. 1. It has to be underlined that the fully equilibrium shape cannot be reached for GBs (as it was, for example, for the surfaces of small Cu crystals [16]). This is due to the fact that the condition of constant crystal volume is not applicable for grains. The grain 1 is similar to the slowly dissolving crystal, and grain 2 is similar to the slowly growing one. Therefore, the ECS for GBs can only be constructed analytically based on the measurements of energy for all GB facets and curved portions (if they are present). One can expect that at the end of the twin plate the next densely packed $\{211\}_1/\{211\}_2$ or $(010)_{CSL}$ facet would appear which is perpendicular to the most densely packed $\{111\}_1/\{111\}_2$ or $(100)_{CSL}$ plane. However, at high temperatures the twins in Cu are not rectangular, unlike those in Au [17]. The facets at the end of twin plates form an angle of 82° with the $(100)_{CSL}$ plane. This 82° facet does not correspond to any low-index CSL plane. The minimum of $\sigma_{GB}(\theta)$ at 82° is due to the formation of a thin GB layer with so-called 9R structure forming a plate of body-centered cubic GB phase in the fcc matrix [18–20]. The $(100)_{CSL}/82°9R$ edges of the twin plates are sharp. AFM reveals only minor corner rounding (less than 1 μm). This feature is reflected in Fig. 3 by the fact that the edges of the ECS $r(\boldsymbol{h})$ are inside of the Wulff plot $f(\boldsymbol{m})$ and do not touch it. This suggests that facets $(100)_{CSL}$ and 9R in Cu remain stable until melting temperature T_m, and their roughening temperatures T_R [$(100)_{CSL}$] and T_R [9R] are higher than T_m.

By decreasing the temperature new facets appear in the ECS of the Σ3 GB. The results are given in Figs. 2 and 4. These additional facets are $\{211\}_1/\{211\}_2$ or $(010)_{CSL}$, $\{100\}_1/\{112\}_2$ or $(110)_{CSL}$, $\{411\}_1/\{111\}_2$ or $(120)_{CSL}$ and $\{522\}_1/\{144\}_2$ or $(130)_{CSL}$. All of them are less densely packed CSL facets than $\{111\}_1/\{111\}_2$ or $(100)_{CSL}$. At $T = 673\ \mathrm{K} = 0.5T_m$ six crystallographically different facets exist simultaneously for Σ3 GB. All observed edges between the facets are sharp. Hence, the new facets appear

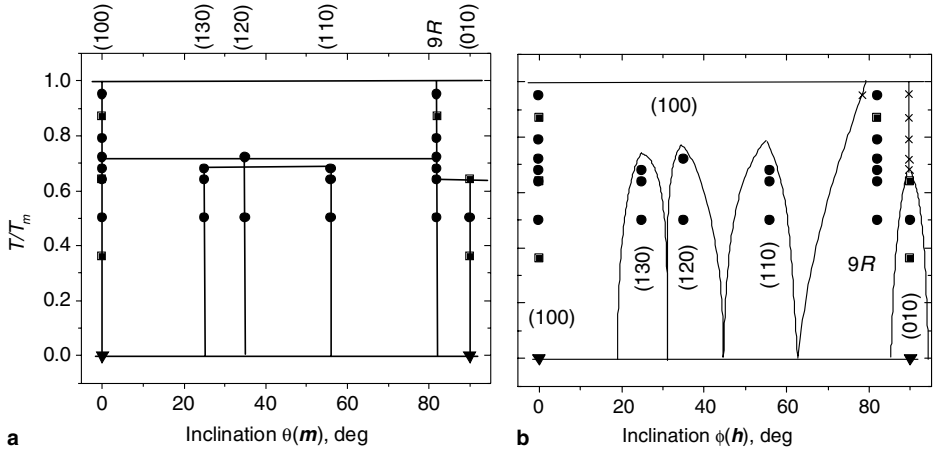

Fig. 4. (a) (T, θ) and (b) (T, ϕ) interfacial stability diagrams for Σ3 {110} tilt GBs in Cu plotted according to the approach [8]. θ and ϕ are angular variables which measure interfacial orientation ($\boldsymbol{m}$) and crystal shape ($\boldsymbol{h}$), respectively, in an equatorial section perpendicular to the {110} tilt axis of the three-dimensional stability diagram. The (T, θ) stability diagram (a) shows positions of cusps in the Wulff plot for $T < T_{Rf}$. The (T, ϕ) stability diagram (b) plots the angular regions for the faceted areas of GB shape. ● and × are experimental data obtained in this work, ■ are experimental data from [18,30–36], ▼ are results of modeling [37]. Only CSL indexes are given in the figure, the respective lattice indexes are: $\{111\}_1/\{111\}_2$ for $(100)_{CSL}$, $\{211\}_1/\{211\}_2$ for $(010)_{CSL}$, $\{100\}_1/\{112\}_2$ for $(110)_{CSL}$, $\{411\}_1/\{111\}_2$ for $(120)_{CSL}$ and $\{522\}_1/\{144\}_2$ for $(130)_{CSL}$.

not at the rough rounded parts of the GB, as observed for surface facets in Pb, Au or He [11,21,22], but at the sharp edges between existing facets. It means that the temperature T_{Rf} when a less densely packed CSL facet really appears in the ECS is lower than the true roughening temperature T_R for this facet. This feature is illustrated schematically in Fig. 3 for the $\{211\}_1/\{211\}_2$ or $(010)_{CSL}$, $\{100\}_1/\{112\}_2$ or $(110)_{CSL}$, $\{411\}_1/\{111\}_2$ or $(120)_{CSL}$ and $\{522\}_1/\{144\}_2$ or $(130)_{CSL}$ facets. At T_R the cusp in $f(\boldsymbol{m})$ appears but it is too shallow to contribute to the ECS, and the $(130)_{CSL}$ facet is metastable. Only when temperature decreases, does the cusp become deep enough, and the metastable facet becomes stable and appears at T_{Rf} in the ECS. At T_{Rf} the plane perpendicular to the radius-vector at the respective cusp in $f(\boldsymbol{m})$ for $(hkl)_{CSL}$ facet touches $r(\boldsymbol{h})$, and the $(hkl)_{CSL}$ facet appears in the equlibrium shape. If we suppose that $\sigma_{hkl}/\sigma_{(100)}$ remains unchanged at low temperatures, we can estimate the values $\sigma_{hkl}/\sigma_{(100)}$ for the less densely packed $(hkl)_{CSL}$ facets from this construction in Fig. 3. The estimated and measured $\sigma_{hkl}/\sigma_{(100)}$ values are given in the Table 1.

According to theory [23,24], the roughening transition is of the Kosterlitz–Thouless type, and should occur at the roughening temperature T_R, given by

$$kT_R = 2\gamma_R d^2/\pi, \quad (1)$$

where k is Boltzmann's constant, γ_R the interface stiffness at T_R, and d the interplanar spacing, i.e., the distance between subsequent crystalline planes, measured in the direction normal to the surface.Neglecting the anisotropy of interfacial tension [23,24] one can substitute the interface stiffness γ_R by σ_{GB}.In the case of the GB one has to use the displacement shift complete lattice [1] and grain boundary shifts lattice [25] to define d, being the height of the elementary step for each CSL facet (Table 1).If one uses for the $\sigma_{(100)}$ the values of stacking fault energy in Cu (5.5×10^{-4} J/m^2 [26] or 7.8 10^{-4} J/m^2 [27] one obtains $T_R = 1.4$–$1.9T_m$ for the $\{111\}_1/\{111\}_2$ or $(100)_{CSL}$ facet in Cu.Using the measured value $\sigma_{9R}/\sigma_{(100)} = 6$ (Fig.3) one obtains from Eq.(1) $T_R = 0.9$–$1.3T_m$ for the 9R facet.It reflects well the fact that $\{111\}_1/\{111\}_2$ or $(100)_{CSL}$ and 9R facets remain in the ECS of $\Sigma = 3$ GB in Cu up to T_m.In other words, the Eq.(1) derived for surface roughening based on the Kosterlitz–Thouless type theory [23,24] is also applicable for GBs.Therefore, using the temperature of actual appearance of each facet T_{Rf} instead of T_R in Eq.(1), one can estimate again the $\sigma_{hkl}/\sigma_{(100)}$ values for the less densely packed $(hkl)_{CSL}$ facets.These data for estimated and measured $\sigma_{hkl}/\sigma_{(100)}$values are also given in Table 1.The discrepancies with the$\sigma_{hkl}/\sigma_{(100)}$ estimations obtained from the Wulff plot could be due to the fact that T_{Rf} is lower than actual (and unknown) T_R. The same $\Sigma3$ GBs behave quite different in other materials [10,28]. Short $(100)_{CSL}$ facets appear close to T_m on the otherwise rough $\Sigma3$ GB in Mo [10]. Four different CSL facets, namely (100), (110), (120) and (210) separated by rough GB portions coexist close to T_m in $\Sigma3$ GBs in Nb [28].

In Fig. 4(a) and (b), the stability diagrams for $\Sigma3$ facets are shown for $\theta(\boldsymbol{m})$ and $\phi(\boldsymbol{h})$ according to the approach proposed in [8] for the ECS. Since all $\Sigma3$ GBs studied were completely faceted, no fields corresponding to the rough phases are present in these diagrams. Vertical lines in Fig. 4(a) indicate the facets in the ECS. Surface or interface orientations between the vertical lines in Fig. 4(a) are unstable to the formation of "hill-and-valley" structure [1] in a dynamic process called "thermal faceting". In other words, if one deliberately produced a plane GB with an intermediate inclination (for example $\theta = 45°$) and annealed it at $T = 0.9T_m$, the GB would decompose into the $(100)_{CSL}$ and 82°9R facets (see Fig. 3(a)), as was observed experimentally in [27–29]. A similar diagram is shown in Fig. 5 for $\Sigma9$ GBs. The increase in the number of stable facets with decreasing temperature is also observed. In Fig. 4(b), the angular areas $\phi(\boldsymbol{h})$ are marked for $\Sigma3$ ECS. The crosses mark the ϕ values where respective facets intersect. The 9R/9R edges lie above T_{Rf} for the $\{211\}_1/\{211\}_2$ or $(010)_{CSL}$ facet at $\phi = 90°$. The position $\phi = 78°$ of $(100)_{CSL}$/9R edge at $T = 1293$ K $= 0.95T_m$ is estimated from the experimentally measured Wulff–Herring diagram (Fig. 3). Unfortunately, at temperatures lower 1200 K, the thermal groove is too shallow and cannot be used for σ_{GB}/σ_{sur} measurements. Therefore, the edge positions for other pairs of facets are shown in Fig. 4(b) only schematically. Another experimental method like chemical or ionic GB etching or GB contact with liquid phase will have to be applied in future in order to construct the Wulff–Herring diagrams for low T.

Table 1
The inclination angles θ, height of elementary step d in units of fcc lattice spacing a and $\sigma_{hkl}/\sigma_{(100)}$ values [measured and estimated from Wulff plot and Eq. (1)] for various $\Sigma3$ CSL facets in Cu

Facet	$\{111\}_1/\{111\}_2$ or $(010)_{CSL}$	$\{211\}_1/\{211\}_2$ or $(010)_{CSL}$	9R	$\{100\}_1/\{112\}_2$ or $(110)_{CSL}$	$\{411\}_1/\{111\}_2$ or $(120)_{CSL}$	$\{522\}_1/\{144\}_2$ or $(130)_{CSL}$	
θ, deg	0	90	82	55	36	25	
d/a	0.86	0.58	0.58	0.42	0.33	0.24	
$\sigma_{hkl}/\sigma_{(100)}$	1 (m)	6.1 (e)	6 (m)	5.1 (e)	5.2 (e)	5.6 (e)	Measured (m) and estimated (e) from Wulff plot (Fig. 2)
$\sigma_{hkl}/\sigma_{(100)}$	1 (m)	0.7 (e)	6 (m)	2 (e)	3.5 (e)	6 (e)	Measured (m) and estimated (e) from Eq. (1)

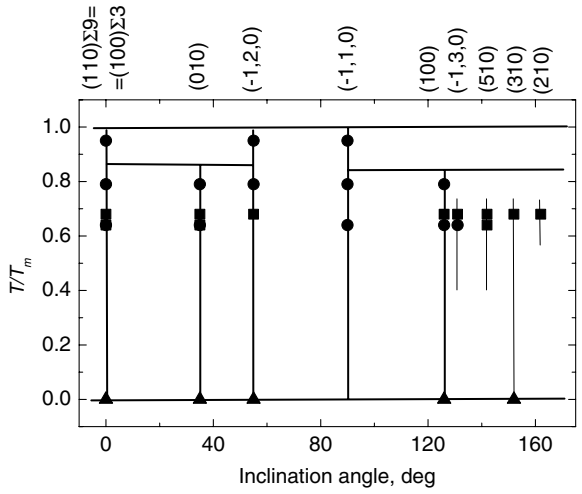

Fig. 5. (T, θ) interfacial stability diagram for $\Sigma 9$ {110} tilt GBs in Cu plotted according to the approach [29] showing positions of cusps in the Wulff plot for $T < T_{Rf}$. ● are experimental data obtained in this work, ■ are experimental data from [35,36,38], ▼ are results of modeling [37]. Only $\Sigma 9$ CSL indexes are given in the figure, the respective lattice indexes are: $\{111\}_1/\{111\}_2$ for $(110)_{CSL}$, $\{144\}_1/\{144\}_2$ for $(010)_{CSL}$, $\{100\}_1/\{447\}_2$ for $(-1,2,0)_{CSL}$, $\{522\}_1/\{111\}_2$ for $(-1,1,0)_{CSL}$, $\{122\}_1/\{122\}_2$ for $(100)_{CSL}$, $\{13,1,1\}_1/\{11,5,5\}_2$ for $(-1,3,0)_{CSL}$, $\{111\}_1/\{1,11,11\}_2$ for $(500)_{CSL}$, $\{755\}_1/\{177\}_2$ for $(310)_{CSL}$, and $\{211\}_1/\{155\}_2$ for $(210)_{CSL}$.

4. Conclusions

1. The cylindrical $\Sigma 3$ and $\Sigma 9$ ⟨110⟩ tilt GBs in a Cu bicrystal, presenting all crystallographically possible inclinations with respect to the ⟨110⟩ tilt axis, become faceted upon annealing between 0.35 and $0.95T_m$.
2. The $\{111\}_1/\{111\}_2$ or $(100)_{CSL}$, $\{211\}_1/\{211\}_2$ or $(010)_{CSL}$, $\{100\}_1/\{112\}_2$ or $(110)_{CSL}$, $\{411\}_1/\{111\}_2$ or $(120)_{CSL}$ and $\{522\}_1/\{144\}_2$ or $(130)_{CSL}$ facets and the non-CSL 82°9R facet are observed for the $\Sigma 3$ GB.
3. The number of facets increase with decreasing temperature and reaches 6 at $0.35T_m$ for the $\Sigma 3$ GB.
4. Wulff–Herring plots, constructed on the basis of GB energy measurements for the various facets (relative to the surface energy, on the basis of thermal groove profile measurement by AFM), for the first time allowed determination of the ECS as a function of temperature.
5. No rough edges (corners) between facets were observed, implying that the roughening temperature T_R for these facets in Cu is higher than the actual appearance temperature T_{Rf}.

Acknowledgement

Investigations were partly supported by INTAS (Contract 03-51-3779) and the Russian Foundation for Basic Research RFBR (Contracts 04-03-34982 and 04-03-32800).

References

[1] Grimmer H, Bollmann W, Warrington DT. Acta Cryst A 1974;30:197.
[2] Tan TY, Sass SL, Balluffi RW. Philos Mag 1975;31:575.
[3] Maksimova EL, Shvindlerman LS, Straumal BB. Acta Metall 1988;36:1573.
[4] Straumal BB, Shvindlerman LS. Acta Metall 1985;33:1735.
[5] Aleshin AN, Prokofiev SI, Shvindlerman LS. Scripta Metall 1985;19:1135.
[6] Hsieh TE, Balluffi RW. Acta Metall 1989;37:2133.
[7] Kim MJ, Cho YK, Yoon DY. J Am Ceram Soc 2004;87:455.
[8] Rottman C, Wortis M. Phys Rev B 1981;24:6274. and 1984;29: 328.
[9] Bo Lee S, Sigle W, Kurtz W, Rühle M. Acta Mater 2003;51: 975.
[10] Straumal BB, Semenov VN, Kogtenkova OA, Watanabe T. Phys Rev Lett 2004;92:196101.
[11] Keshishev KO, Parshin AYa, Babkin AV. Sov Phys JETP 1981;53:362.
[12] Straumal BB, Polyakov SA, Bischoff E, Gust W, Mittemeijer EJ. Interf Sci 2001;9:287.
[13] Schölhammer J, Baretzky B, Gust W, Mittemeijer E, Straumal B. Interf Sci 2001;9:43.
[14] Mullins WW. Metal surfaces. Metals Park (OH): Amer. Soc. Metals; 1962. p. 17.
[15] Schoellhammer J, Chang L-S, Rabkin E, Baretzky B, Gust W, Mittemeijer EJ. Z Metallkd 1999;90:687.
[16] Chatain D, Ghetta V, Wynblatt P. Interf Sci 2004;12:7.
[17] Goodhew PJ, Tan TY, Balluffi RW. Acta Metall 1978;26:557.
[18] Wolf U, Ernst F, Muschik T, Finnis MW, Fischmeister HF. Philos Mag A 1992;66:991.
[19] Ernst F, Finnis MW, Hoffmann D, Muschik T, Schönberger U, Wolf U. Phys Rev Lett 1992;69:620.
[20] Hofmann D, Finnis MW. Acta Metall Mater 1994;42:3555.
[21] Heyraud JC, Metois JJ. Acta Metall 1980;28:1789. and J Cryst Growth 1980;50:571.
[22] Heyraud JC, Metois JJ. Surf Sci 1983;128:334.
[23] Fisher DS, Weeks JD. Phys Rev Lett 1983;50:1077.
[24] Nozieres P, Gallet F. J Phys (Paris) 1987;48:353.
[25] Rybin VV, Perevesentsev VN. Sov Phys Sol State 1975;17:2103.
[26] Gallagher PCJ. Met Trans 1970;1:2429.
[27] Murr E. Interfacial phenomena in metals and alloys. Reading (MA): Addison Wesley; 1975.
[28] Straumal BB, Semenov VN, Khruzhcheva AS, Watanabe T. J Mater Sci 2005;40:871.
[29] Andreev AF. Sov Phys JETP 1981;53:1063.
[30] Muschik T, Laub W, Finnis MW, Gust W. Z Metallkd 1993;84: 596.
[31] Muschik T, Laub W, Wolf U, Finnis MW, Gust W. Acta Metall Mater 1993;41:2163.
[32] Laub W, Oswald A, Muschik T, Gust W, Fournelle RA. In: Johnson WC, editor. Solid–solid phase transformations. Warrendale (PA): The Minerals, Metals & Materials Society; 1994. p. 1115.
[33] Oswald A, Laub W, Gust W, Fournelle RA. In: Johnson WC et al., editors. Solid–solid phase transformations. Warrendale (PA): The Minerals, Metals & Materials Society; 1994. p. 1121.
[34] Ernst F, Finnis MW, Koch A, Schmidt C, Straumal B, Gust W. Zt Metallkd 1996;87:911.
[35] Forwood CT, Clarebrough LM. Acta Metall 1984;32:757.
[36] Clarebrough LM, Forwood CT. Phys Stat Sol a 1980;60:51.
[37] Merkle KL, Wolf D. Philos Mag A 1992;65:523.
[38] Sukhomlin GD, Andreeva AV. Phys Stat Sol a 1983;78:333.